Page Proof Instructions and Queries

Thank you for choosing to publish with us. This is your final opportunity to ensure your article will be accurate at publication. Please review your proof carefully and respond to the queries using the circled tools in the image below, which are available **by clicking "Comment"** from the right-side menu in Adobe Reader DC.*

Please use *only* the tools circled in the image, as edits via other tools/methods can be lost during file conversion. For comments, questions, or formatting requests, please use $\boxed{T}$ Please do *not* use comment bubbles/sticky notes 💬.

| Comment ▾ | 💬 ✏️ T ⊤ ⊤ T₄ T ⊤ ✏️ 🧽 🔖▾ 📎▾ ⟁▾ |
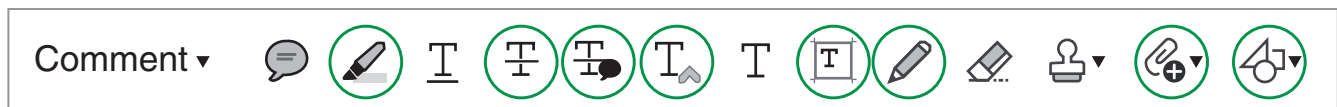
*If you do not see these tools, please ensure you have opened this file with Adobe Reader DC, available for free at get.adobe.com/reader or by going to Help > Check for Updates within other versions of Reader. For more detailed instructions, please see us.sagepub.com/ReaderXProofs.

No.	Query
	Please note, only ORCID iDs validated prior to acceptance will be authorized for publication; we are unable to add or amend ORCID iDs at this stage.
	Please confirm that all author information, including names, affiliations, sequence, and contact details, is correct.
	Please review the entire document for typographical errors, mathematical errors, and any other necessary corrections; check headings, tables, and figures.
	Please confirm that the Funding and Conflict of Interest statements are accurate.
	Please ensure that you have obtained and enclosed all necessary permissions for the reproduction of artistic works, (e.g. illustrations, photographs, charts, maps, other visual material, etc.) not owned by yourself. Please refer to your publishing agreement for further information.
	Please note that this proof represents your final opportunity to review your article prior to publication, so please do send all of your changes now.
AQ: 1	Please provide name of the department in the affiliation.
AQ: 2	Please insert an in-text citation for Figure 8.
AQ: 3	Please provide page range in ref. 1.
AQ: 4	Please provide volume number and page range in ref. 10.
AQ: 5	Please provide complete details or a URL in ref. 13.
AQ: 6	Please provide abbreviated form of journal name in ref. 15.
AQ: 7	Please provide complete details or a URL in ref. 19.

Validation of an in-house-designed tensile testing machine for the mechanical characterization of 3D-printed specimens

Francesca Cosmi [iD] and Alberto Dal Maso

Abstract

Additive manufacturing is gaining greater and greater popularity in recent years: thanks to a dramatic reduction of costs and increasing print quality, more and more people are attracted to 3D printing, even for the production of end-use load-bearing parts. Today, there are no universally accepted norms that guide the engineer through the uncertain task of predicting the mechanical behavior of 3D-printed parts. Even though there are numerous reports and articles in literature regarding this topic, the designer will have to rely mostly on his own mechanical tests. This paper describes the design of an in-house-built machine for 3D-printed material tensile testing. The accuracy of this test-rig has been verified through comparison of results on different 3D-printed specimens: these were realized through fused deposition modelling (FDM) and were divided into four distinct sets, based on the material and their orientation on the buildplate. Some samples were printed in PLA, others in XTCF-20^{TM}: a composite material made of a matrix of Amphora^{TM} polymer reinforced with 20% in weight carbon short fibers. PLA samples were printed flat on the buildplate, on one side and standing: this affects directly the orientation of the plastic fibers. Tensile tests were performed both on ours and on a high-end commercial testing machine, following the ISO 527 norm. Maximum stress, strain at maximum stress and Young's modulus were calculated for each tested specimen: these measures allowed to compare the results of the two testers. Results proved coherent, thus validating the in-house machine, which was realized for a fraction of the cost of an equivalent commercial model.

Keywords

3D printing, FDM, tensile, mechanical characterization, additive manufacturing, testing machine

Date received: 17 October 2018; accepted: 23 April 2019

Introduction

Three-dimensional (3D) printing finds numerous applications in the field of engineering: its growing popularity and the dramatic reduction in costs are opening doors to countless new opportunities, not only in terms of research but also in medium-scale production of load-bearing applications.[1,2] A great choice of materials and composites is available to engineers and "makers," and new ones are being synthetized and commercialized every day. Predicting the mechanical properties of a 3D-printed part is not a trivial task: many authors attempted to develop methods for this,[3–10] emphasizing that mechanical behavior depends very much on the specific printer used and on a huge variety of other printing parameters, which rarely coincide with each designer's specific setup. Therefore, in the end, tensile tests need to be carried out for each machine configuration used, in order to gain the greatest possible knowledge over the mechanical characteristics of the specific

3D-printed part. This can be done on commercial tensile testing machines, but most makers or small companies might not be able to afford such an expensive apparatus.

Fused deposition modelling (FDM) is the cheapest and most widespread 3D printing technology on the market and it is well known that, in parts printed with this technique, mechanical characteristics along the x/y axes differ greatly from those along the z axis.[8,10] More generally, mechanical properties vary depending on the raster orientation angle. Deng et al.[11] presented a method to predict ultimate tensile strain (UTS) in specimens printed at a certain angle θ once the UTS of flat-built ($\theta = 0°$),

University of Trieste, Trieste, Italy [AQ1]

DIA - Department of Engineering and Architecture

Corresponding author:
Francesca Cosmi, University of Trieste, Via A. Valerio I, Trieste TS 34127, Italy.
Email: cosmi@units.it

standing-built ($\theta = 90°$) and 45°-built specimens is known (Figure 1). These data, however, depend on a wide variety of other factors, including material, printer type and brand, filament manufacturer, layer height, printing temperature just to name a few. More and more 3D-printing materials are being produced every day, however technical datasheets are often vague and lacking important information. Since the properties of bulk materials (generally obtained through injection molding) can be very different from those of the same material when 3D-printed, the need to personally test the materials used for 3D-printed design is evident. There are several articles in literature comparing the bulk mechanical properties of the most popular FDM materials and those of the corresponding 3D-printed part, in relation with the aforementioned parameters;[3,5–7,9,12] however, these are often limited to the most common materials (PLA, ABS, Nylon). Attempts have been made to improve mechanical resistance through optimization algorithms,[4] but the parameters involved are so numerous that such studies cannot be considered universally valid for each and every possible 3D-printing

Figure 1. Different printing orientations.

configuration. Therefore, on principle, tensile tests should be carried out for the specific printing configurations used, in order to gain the greatest possible knowledge over the mechanical characteristics of the materials and settings employed.

This can be done on commercial tensile testing machines, which can be bought for about €20,000, but most makers or small companies might not be able to afford such an expensive apparatus. This paper describes the design of an in-house-built machine for 3D-printed material tensile testing at a fraction of the cost. The designed tester is the simplest possible: a rigid frame, two vise-grips, an extensometer and a load cell; the system is mechanically hand-driven. Tensile tests were performed on ISO 527 standard specimens both on this machine and, parallel, on a certified MTS™ tester. Results were then compared in order to validate the in-house-designed machine. Tests were carried out on 3D-printed specimens, which were realized with a Builder Premium™ FDM 3D printer. Stress–strain curves were obtained and analyzed for each sample; from these curves, ultimate tensile strength, strain at maximum stress and Young's modulus were calculated and served as reference for the validation process.
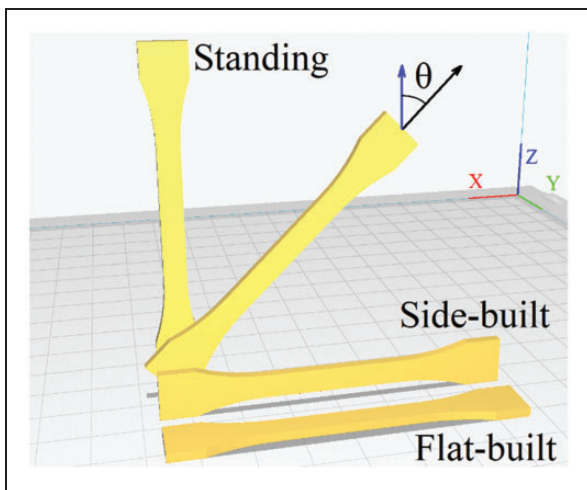
Materials and methods

Tensile tests were performed following the ISO 527 norm: "Plastics: determination of tensile properties."[13] The specimen type 1BA was chosen at first, and the machine was designed specifically for this particular geometry. This does not prevent it from working on different kinds of samples, however it is optimized for this type of specimens.

Geometry of the specimens

The geometry of the specimens used is shown in Figure 2, while the dimensions which were chosen are listed in Table 1. The norm suggests a gauge length (L_0) of 50 mm; however, shorter gauge lengths
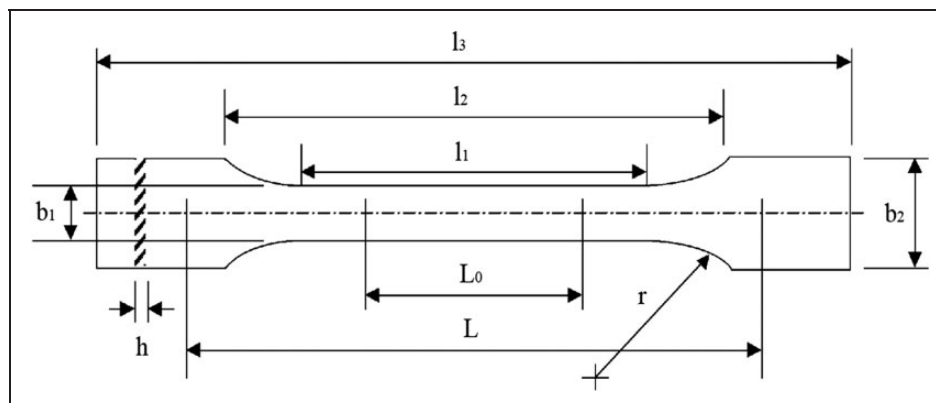

Figure 2. Geometry of the specimens chosen for the tensile tests.

Table 1. Dimensions (in mm) of the specimens chosen for the tensile tests.

l_3	l_2	l_1	b_2	b_1	h	L_0	L	r
73	58	30	10	5	2	25	58	40

of 25 mm are accepted as well. Due to time and material availability, which may be an issue to many makers, the latter option was chosen.

Specimens were 3D-printed using a Builder™ Premium Medium™ FDM printer. All settings were controlled through the freeware slicer Ultimaker™ Cura™. Wherever necessary, supports were added to allow the print of overhanging areas and manually removed before testing.

Design of the machine

The procedure we followed to build the machine is described in the following paragraphs. This tensile tester was originally designed to apply small loads during micro-CT acquisitions on ASTM type D1822 samples.[14] It has been later adapted to comply with ISO 527 standards and specimen geometry.

Description of the system. The machine consists of two caps which are mounted on the opposite ends a stiff cylindrical frame. On the lower end, a grip is mounted on a platform. A load cell is positioned on the support connecting the platform to the frame, in order to measure the applied force (F).

The upper cap hosts the mechanism through which the displacement is applied. A threaded hole in the center of the cap couples with a hand-driven screw: this screw is connected to the other grip, so that as the screw revolves, the grip translates vertically. To avoid unwanted torsion, the orientation of the moving grip is kept parallel to the lower one via two fixed pins that slide into two corresponding holes of the grip. The coupling between the screw and the grip is designed so that the revolution of the screw is allowed, while their relative translation is not. An extensometer measures the distance between the cap and the grip. Figure 3(a) shows an exploded CAD drawing of the whole system.

Upper and lower cap. The caps were manufactured in a standard aluminum alloy through turning. Both caps have a deep engraving that couples with the frame, holding it in place. Four screws per cap guarantee a precise positioning.

Grips. The ISO 527 norm specifies that grips should preferably be wedge-type, so as to obtain a self-tightening during the test: this is the most secure kind of grip. However, the norm allows also vise-type grips, which are fastened manually through a screw at the beginning of each test. With this kind of grips, the

operator must predict the maximum load on the specimen and tighten the screws accordingly. The main advantage is a much greater simplicity in the mechanism, which is therefore easier to build. For this reason, screw-driven vise grips were chosen for the machine.

Figure 4 shows the geometry of the grips. Each grip consists of a U-shaped rigid structure, a fixed plate and a moving plate. The fixed plate is secured on one side of the structure, while the moving plate is placed on the opposite side. The specimen is inserted in between the plates. A hexagonal M6 screw presses the moving plate toward the specimen: the resulting pressure guarantees a tight fastening. To avoid twisting of the moving plate, two fixed pins are coupled with two corresponding holes on the part.

The lower grip is fixed to the lower cap with two screws. The upper grip is coupled with the displacement screw via a revolute joint: the revolution of the screw is allowed, while all relative translations (in particular vertical motion) are not permitted. In this way, the translation of the screw is transferred to the upper grip.

All these parts are built in steel and were obtained using an in-house milling machine.

Sensors. The measure of force is obtained with a load cell, which is placed on an elastic metal support connected to the lower grip.

The measure of displacement is obtained with an extensometer. The instrument is fixed on the upper cap, while the mobile probe is connected to the upper grip. The extensometer has a spring that guarantees contact with the grip. Table 2 summarizes the main technical specifications for the acquisition system, while Figure 3(b) shows the assembled tester.

Data elaboration

The acquired data are elaborated by a computer program to obtain stress and strain values. Stress is calculated given the measured force (F) and the sample's minimum section area ($A = 10$ mm^2)

$$\sigma = F/A \tag{1}$$

Nominal strain is evaluated given the displacement measurement (ΔL) and the distance between grips on the specimen ($L = 58$ mm)

$$\varepsilon_t = \Delta L/L \tag{2}$$

The nominal strain does not represent, in general, the actual strain of the material inside the specimen, due to the non-uniform cross section of the tested samples, which are wider on each end. This causes a non-uniform distribution of tension inside the specimen, which is not uniaxial, leading to a systematic error. The actual strain is much better represented
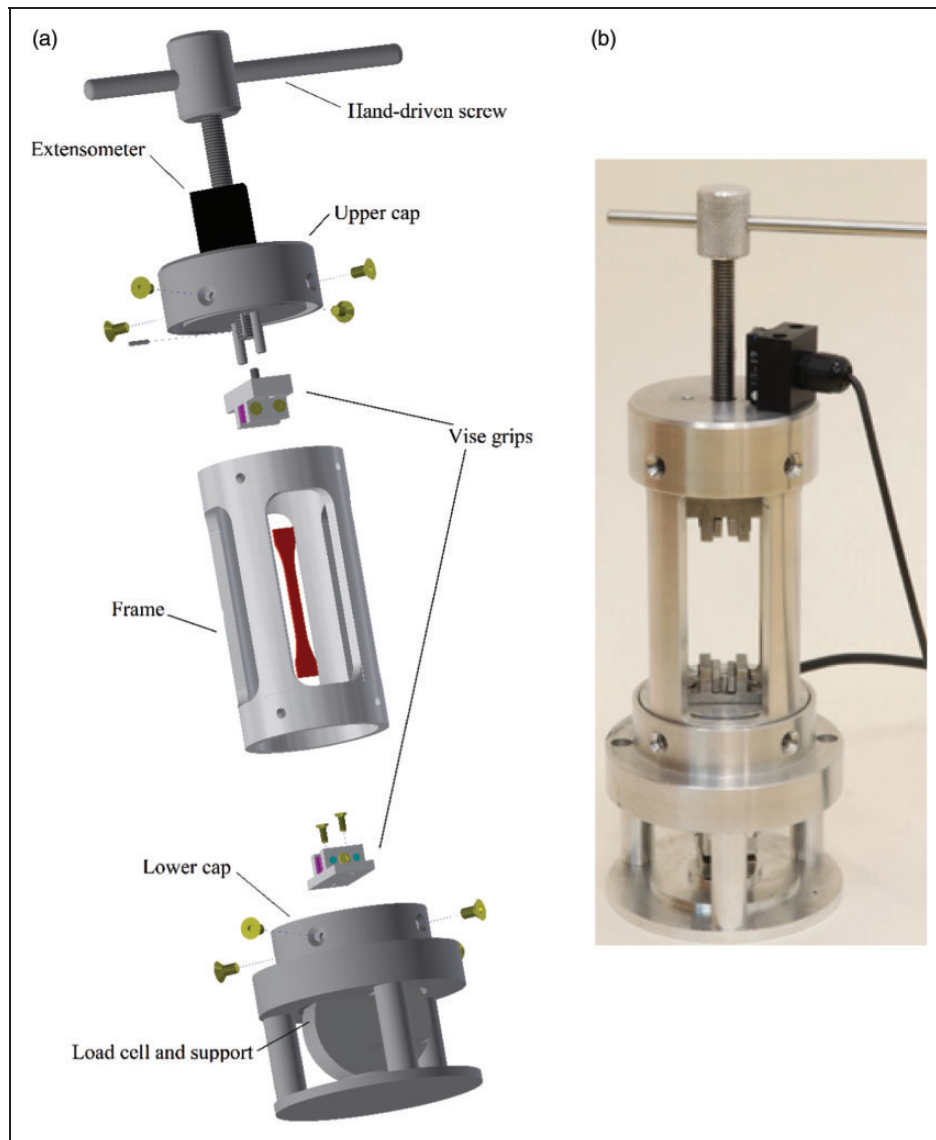
Figure 3. (a) Exploded view of the designed testing machine; (b) the assembled device.
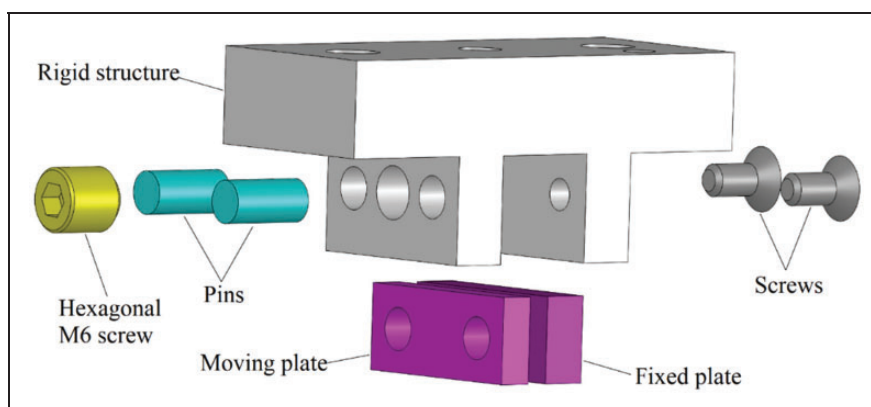

Figure 4. Exploded view of the designed vise grips.

by the strain at gauge length (ε_{gl}), defined as

$$\varepsilon_{gl} = \Delta L_0 / L_0 \qquad (3)$$

This can be measured with a clip-on extensometer, or with more expensive optical devices. If these instruments are not available, the measure of displacement on the grips can be used, as long as the resulting strain

is multiplied by a correction factor that considers the non-uniformity of stress and strain distribution.

To predict the ratio between ε_t and ε_{gl}, an FEM elastic linear analysis was carried out on a virtual specimen using Autodesk$^{\text{TM}}$ Inventor's simulation package. A custom material with Young's modulus of $E = 2$ GPa and Poisson's ratio $\nu = 0.36$ was assigned, since these values are close to those of most common 3D-printed polymers. A force $F_1 = 100$ N was applied parallel to the axis of the sample. Thanks to symmetry, only half of the specimen was studied. By measuring the displacement on the gauge length (equation (3)) we obtain

$$\varepsilon_{gl} = \frac{0.125\,\text{mm}}{25\,\text{mm}} = 5 \times 10^{-3} \tag{4}$$

Instead, by measuring the displacement on the grips (equation (2)) we obtain

$$\varepsilon_t = \frac{0.253\,\text{mm}}{58\,\text{mm}} = 4.48 \times 10^{-3} \tag{5}$$

Therefore, by measuring the displacement on the grips instead of the gauge length, for this particular specimen geometry one commits an error calculated as

$$e = \frac{\varepsilon_{gl} - \varepsilon_t}{\varepsilon_{gl}} = 10.3\% \tag{6}$$

Note that the numerical values assigned to E and to F_1 are arbitrary: the value of e depends solely on the geometrical characteristics of the specimen and Poisson's ratio. Several equivalent simulations were performed applying a different force $F_2 = 200$ N and the resulting error e was exactly the same. In further simulations, the Poisson's ratio was varied in a range from 0.3 to 0.39: the resulting calculated displacements shifted by a maximum of 0.2%, which is negligible, therefore the result can be considered independent from the Poisson's ratio.

A mesh-convergence study was carried out on the part: results are shown in Figure 5(a) and (b). The average element size is not absolute, but is expressed as a fraction of the half-specimen length, that is 12.5 mm. From the plot, it can be observed that all the measures of interest immediately converge to their stable value.

In conclusion, to obtain an accurate reading of strain measuring the displacement on the grips instead of on the gauge length, the following corrected formula must be adopted

$$\varepsilon = \frac{1}{1 - e}\varepsilon_t = 1.116 \times \frac{\Delta L}{L} \tag{7}$$

The stress and strain readings obtained in-house can be now compared to those obtained in the MTS$^{\text{TM}}$ lab and this procedure can be experimentally validated.

Tests on 3D-printed specimens

Several specimens were 3D printed, in order to test and validate the efficiency and the reliability of the newly designed testing procedure. Some were tested in-house while others were tested in MTS$^{\text{TM}}$ laboratories. In order to compare the two sets of data, all the parameters which may have an effect on the results were monitored and kept constant as far as possible.

Table 2. Technical specifications for the in-house tensile testing machine.

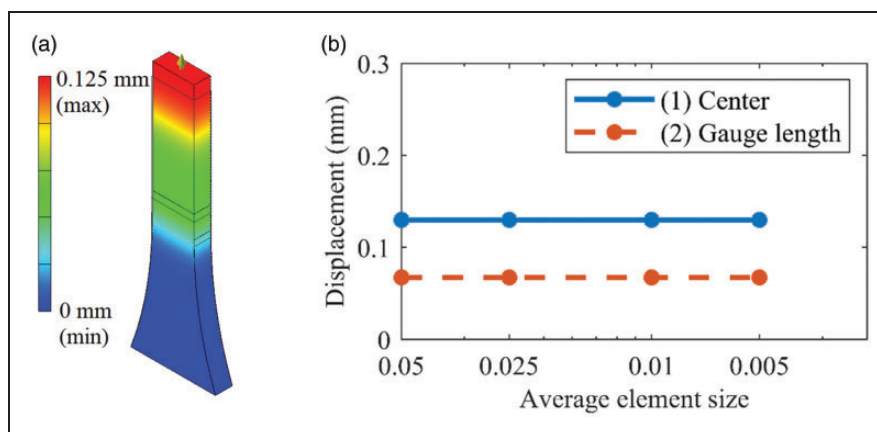| In-house machine	Displacement measure	Force measure
Instrument	Linear position sensor	Load cell
Full scale	10 mm	800 N
Resolution	0.005 mm	1.3 N
Acquisition frequency	1 Hz	1 Hz

Figure 5. (a) FEM simulation results: displacement along the z axis; (b) mesh convergence study referred to the displacement value (1) at the center of the specimen and (2) at one end of the gauge length. Results evidently converge.

Moreover, a univocal procedure was defined to quantify the closeness of the data sets.

Parameters involved. Two materials were studied: PLA (poly lactic acid) by Builder™ and XTCF-20™ by ColorFabb™. PLA is a biodegradable, non-toxic polymer, very popular for FDM applications.[15–17] Its relatively low glass transition temperature (65 °C) and its low cost make it one of the first choices among 3D printing enthusiasts. Bulk PLA has a tensile strength that ranges from 50 to 80 MPa, depending on a series of production parameters that vary from one specific manufacturer to the other. These values are relatively high, making PLA a fair choice for certain structural applications. 84 specimens were printed in PLA for this study.

XTCF-20™ is a composite material by ColorFabb™ made of a matrix of Amphora™ polymer reinforced with 20% in weight carbon short fibers. Amphora™ is a less common 3D printing material, originally developed by Eastman™ (Kingsport, TN, USA), a large chemical company. The exact chemical composition of this polymer is not published by the manufacturer. Bulk Amphora™ has a tensile strength of 50 MPa, slightly lower than most PLAs, and its recommended printing temperature is 250 °C, which is slightly higher than that of PLA. ColorFabb™ states that the short carbon fibers mixed in the matrix increase the ultimate tensile strength and the stiffness of XTCF-20 composite.

Mechanical resistance of 3D-printed parts depends greatly on the orientation of the filament fibers, which is strictly connected to the specimen's orientation on the buildplate. It is well known that the resistance in the direction orthogonal to the layers is generally inferior to the resistance parallel to the fibers. To quantify this effect, some specimens were printed flat on the buildplate, some on one side ($\theta = 90°$), others standing ($\theta = 0°$).

There are many other parameters that control a print and, more or less indirectly, the mechanical characteristics of the parts produced: for example layer height, print speed, extruder temperature, etc. These have not been investigated in this study and their value has been fixed as reported in Table 3.

Young's modulus. Defining Young's modulus from the data obtained in a tensile test is not a univocal task, especially when dealing with plastics or, in general, with non-linear materials. ISO 527 norm suggests one standard method to calculate the modulus. Let us consider the $\sigma - \varepsilon$ plot of a certain specimen, where each point $(\sigma(t), \varepsilon(t))$ represents a reading at a certain instant t. The norm defines the modulus of the material E as the slope of the regression line of the points with ε in between $\varepsilon_1 = 0.05$ % and $\varepsilon_2 = 0.25$ %.

In order to obtain a significant amount of points in this interval (i.e. at least 10), the elongation speed v

Table 3. Main printing parameters fixed for all tests.

	PLA	XTCF-20
Layer height	0.2 mm	0.2 mm
Wall thickness	4 mm	4 mm
Top/bottom thickness	0.8 mm	0.8 mm
Infill density	100%	100%
Infill pattern	Square grid	Square grid
Flow	100%	100%
Extruder temperature	215 °C	250 °C
Preheated bed temperature	60 °C	70 °C
Print speed	50 mm/s	30 mm/s
Travel speed	100 mm/s	60 mm/s

must be adjusted according to the formula given by the norm

$$v = \frac{fLr}{L_0} \tag{8}$$

where:

f is the frequency of acquisition;

r is the resolution of the measuring instrument;

L and L_0 as previously defined, respectively distance between grips and gauge length of the sample.

By inserting the numerical values of the available testing machine, we obtain a maximum recommended speed of 0.66 mm/min, which corresponds to an elongation rate of $2 \times 10^{-4} s^{-1}$.

When examining polymeric materials, it is not always easy to define a yield point or a rupture point. Sometimes the specimen reaches failure in a fragile manner, other times material flow occurs: that is when certain areas of the specimen extend indefinitely, behaving as high-viscosity liquids, without reaching an actual breaking point. In this study, only the maximum stress (σ_{max}) and the corresponding strain (ε_{max}) are considered.

Validation of results

In order to validate the procedure described in the section Data elaboration, some specimens were tested in MTS laboratories while other equivalent ones were tested in-house. The comparison of results was performed on three quantities: maximum stress, maximum strain and Young's modulus. For in-house tested samples, the strain was corrected according to equation (7).

The samples which were sent to MTS™ were tested on a Synergie 200™ machine, of which the main technical specifications are reported in Table 4. On this tester, the displacement was measured directly on the gauge length of each specimen. In this case, by applying equation (8), we obtain that the maximum acceptable strain rate is $1.2 \times 10^{-2} s^{-1}$, definitely

higher than for the other machine. During the tests, a much lower strain rate was actually applied, in order to maintain the displacement speed as close as possible to that of the in-house machine.

Results

A total of 103 samples were tested, of which 30 in MTS^{TM} laboratories and 73 in-house. The main results are presented in the following paragraphs.

Table 4. Technical specifications for the MTS^{TM} testing machine.

Synergie 200^{TM} machine	Displacement measure	Force measure
Instrument	Extensometer	Load cell
Full scale	0.24 mm	1000 N
Resolution	1e-4 mm	0.02 N
Acquisition frequency	50 Hz	50 Hz

Test results

As previously stated, the mechanical characteristics of 3D-printed samples depend on their orientation on the buildplate, therefore results are presented separately for each orientation. The plots of Figure 6 show the stress–strain curves for PLA samples printed flat, side and standing and for XTCF-20 samples. Blue curves refer to in-house tested samples while red curves refer to MTS^{TM}-tested ones. Table 5 summarizes the main statistical results for this set.

MTS^{TM} measures contain many more points, being the acquisition frequency definitely higher. Moreover, the $\sigma - \varepsilon$ curve presents a large perfectly linear segment, which does is not so evident in-house-tested specimens. Presumably, this depends on the displacement speed, which is more uniform in the motor-driven system than in the hand-driven machine. Considering that the stress reading depends also on acquisition time, a non-uniform speed introduces fluctuations in the measure.

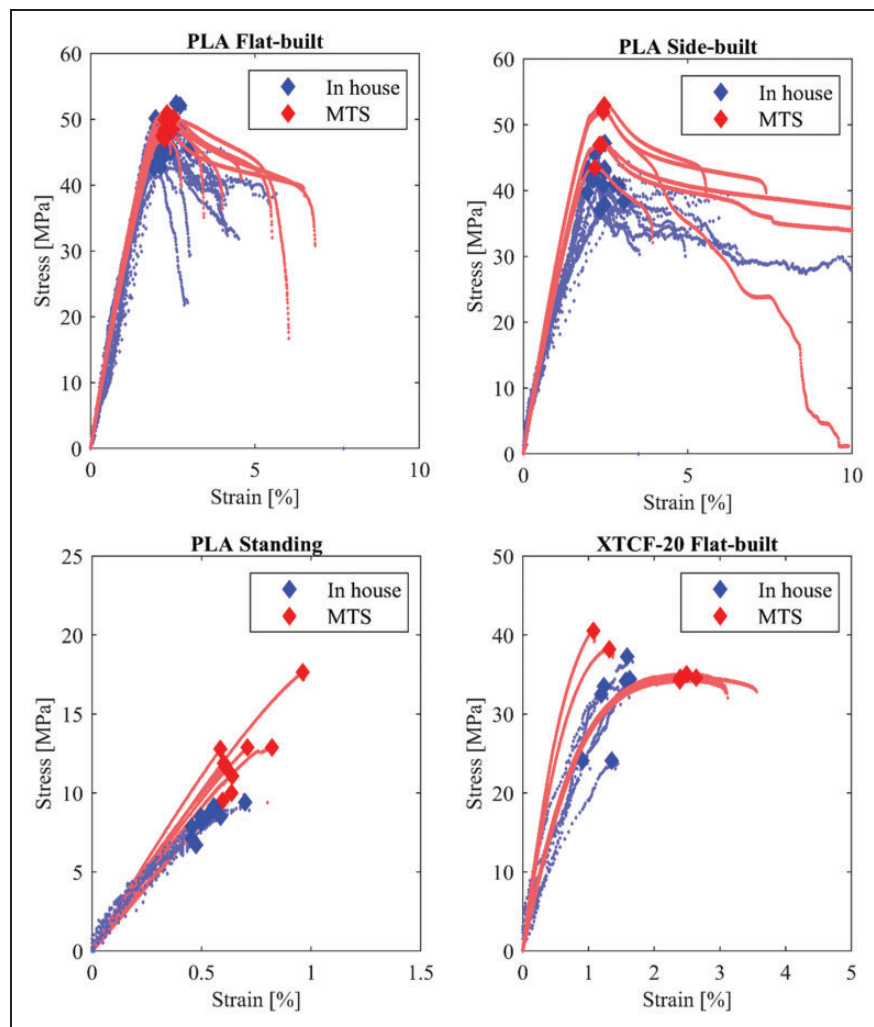Standing specimens are fragile, therefore the maximum stress and breaking load coincide.


Figure 6. Stress–strain curves obtained for all tested samples. Different colors highlight different testing machines.

Table 5. Main results for PLA and XTCF-20. CV indicates the coefficient of variance for each set.

	Flat-built		Side-built		Standing		XTCF-20	
	house	MTS	house	MTS	house		house	MTS
No. of tested specimens	26	9	18	6	9	9	7	6
Max stress, MPa	47.22	49.19	41.76	49.10	8.21	12.26	31.4	36.20
(CV)	(5.13%)	(2.86%)	(6.07%)	(7.90%)	(10.8%)	(19.3%)	(16.6%)	(7.11%)
Strain at max stress, %	2.29	2.33	2.36	2.36	0.53	0.68	1.35	2.05
(CV)	(11.7%)	(5.21%)	(13.6%)	(4.34%)	(14.8%)	(18.7%)	(19.4%)	(32.8%)
Young's Modulus, GPa	2.52	2.97	2.88	2.89	1.67	1.93	2.92	4.27
(CV)	(21.6%)	(3.01%)	(26.5%)	(6.2%)	(19.4%)	(9.77%)	(23.2%)	(23.8%)
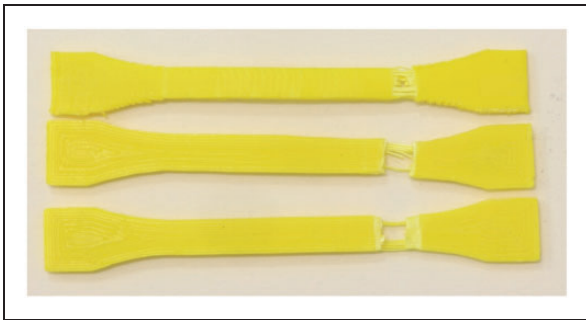
Figure 7. Examples of flow on some PLA specimens.

The specimens printed in the other two orientations behave differently. At first there is an approximately linear increase of the stress with the strain; then, around the maximum stress point, there is a gradual inversion of the slope and as strain increases, the measured stress decreases. Sometimes this phase lasts until reaching the full scale of the machine, without failure occurring. This phenomenon is common to many plastics and is often referred to as "flow": the material behaves substantially as a fluid and flows to allow the displacement. This phenomenon occurs rarely on the whole cross section: usually only some fibers exhibit flow, while others break sooner. Figure 7 shows examples of flow on some PLA specimens.

As expected, the mechanical characteristics of samples printed standing are substantially different from those of flat-built and side-built specimens. Ultimate strength is about four times lower than the other two groups. Even the elastic modulus is inferior, though not to the same extent. There is a slight difference between flat-built and side-built samples: the formers are somewhat less resistant, but their Young's modulus is practically identical. In both cases, in fact, the fibers are oriented parallel to the force, therefore they offer the maximum resistance. The carbon-reinforced specimens exhibit a maximum stress that is definitely inferior to that of pure PLA, contrary to expectations. Its Young's modulus is slightly greater than that of PLA, while strain at maximum stress is smaller. This material behaves in a fragile manner and flow never occurs.

Result comparison and process validation

It is now possible to compare the results obtained with the certified MTS^{TM} machine and those obtained with the newly designed apparatus. In particular, it is important to compare the values of strain at maximum stress (ε_{max}), in order to validate the reading of ε, obtained through the previously described procedure.

To decide whether a set of in-house measurements is compatible with the MTS^{TM} corresponding ones, a T-test was performed. For this study, the null hypothesis H_0 can be expressed as: "There is no significant difference between the in-house measurements and the MTS measurements." This statement is to be proven right or wrong (meaning there is a significant statistical difference between in-house and MTS tests) to the level of significance p. If p is small (generally <0.01) then there is a high likelihood that the in-house measurements are statistically different from the MTS ones. On the other hand, if $p > 0.05$, there is no evidence to support that there is a significant difference between the two sets of data, therefore they are considered compatible. If $0.01 < p < 0.05$, the significance level is neither high nor low, therefore no ultimate statement can be made in this threshold area. The T-test was performed for maximum stress, strain at maximum stress and Young's modulus and for each printing orientation and material.

There are no grounds to assume that the populations have, in general, equal variances: therefore, an F-test was performed first, to determine whether T-test should take this into account. If the F-test is positive, meaning that there is a significant difference between the two variances within the 5% threshold, then an unequal-variance T-test was performed, using Satterthwaite's approximation.[18] Results of the T-test are summarized in Table 6.

Each data set is graphically represented in Figure 9 by its mean value μ and error bars, where the length of error bars is equal to the standard deviation SD ($SD = CV \times \mu$).

The T-test helps understand if there is or there is not a statistical difference between the two measuring methods, however it does not give information on

Table 6. Results comparison between in-house and MTS measurements: T-test and p-value.

	Flat-built	Side-built	Standing	XTCF-20
Max stress, MPa	Different	Different	Different	Compatible
(CV)	(p = 0.007)	(p = 0.004)	(p = 0.001)	(p = 0.061)
Strain at max stress, %	Compatible	Compatible	Different	Threshold
(CV)	(p = 0. 0.668)	(p = 0.998)	(p = 0.008)	(p = 0.027)
Young's modulus, GPa	Different	Compatible	Threshold	Threshold
(CV)	(p = 0.020)	(p = 0.970)	(p = 0.044)	(p = 0.024)
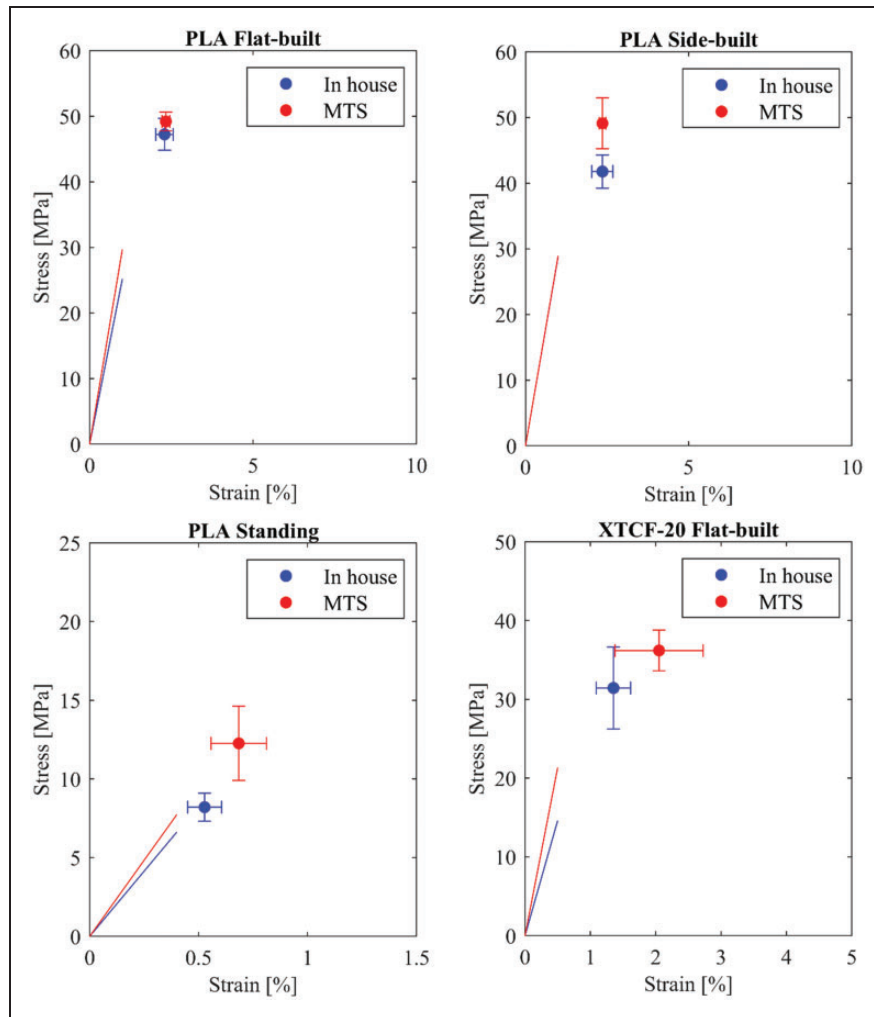
Figure 8. Mean values and error bars for each group. Lines from origin indicate modulus [AQ2].

how big the difference is. A discussion about the relative errors of the in-house measurements follows here.

For XCTF-built samples, only the strain at maximum stress results are fully compatible. However, the relative error between the mean values of Young's modulus is 15%. Similarly, for maximum stress, the error is merely 4%.

Side-built samples show excellent correspondence, except for maximum stress, where the error is again 15%.

XTCF-20 samples show good correspondence for maximum stress, while strain at maximum stress and

Young's modulus are in the threshold: more tests would be necessary to confirm the compatibility of results for these measurements.

Standing-built samples show the greatest errors, which are most likely due to the many sources of variability which occur when 3D-printing such thin vertical features.

For each category, the in-house machine on average provided smaller values. This effect is likely due to the elongation rate: MTS[TM] tests were performed at a constant strain rate of 0.1%/s (corresponding to 1.5 mm/min) in the first 20 s and 0.3%/s
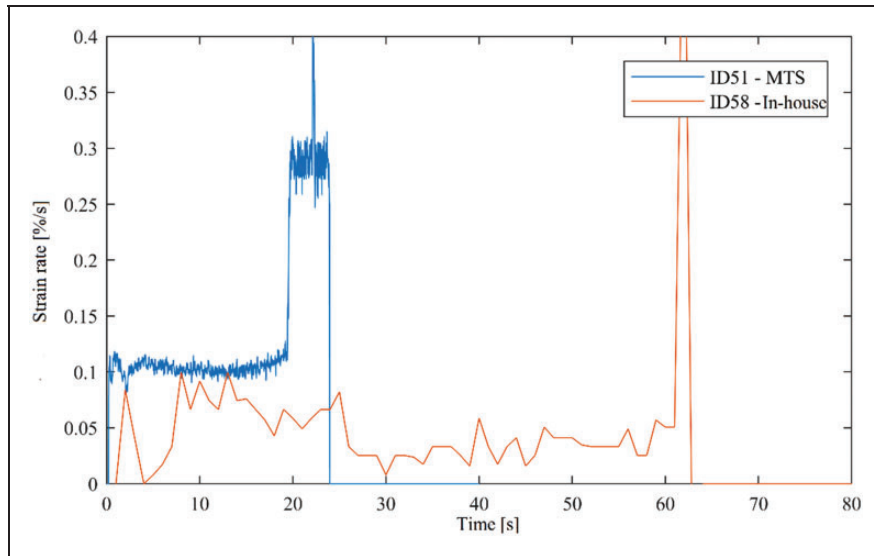
Figure 9. Instantaneous strain rate plotted versus time for one example specimen tested by MTS[TM] (blue) and one tested in-house (red).

(4.5 mm/min) after. In-house tests were hand-driven, therefore it was impossible to maintain a constant speed: strain rate was on average equal to 0.05%/s. It is not infrequent that mechanical properties of plastic materials are strongly affected by strain rate, exhibiting higher tensile strengths at faster speeds.[19] The lower strain rate and the large fluctuations in elongation speed of the in-house tests explain both the systematic error in the stress readings and the non-linearity of these measures. As an example, Figure 9 shows the strain rate of one MTS[TM]-tested sample plotted versus time throughout the test, compared with that of one in-house-tested specimen. The fluctuations in strain rate for the latter are evident.

Conclusions and future developments

When testing 3D-printed polymeric materials, the sources of variability are numerous: non-homogeneity of the filament deposition, slight differences in test piece preparation, age of the specimen all contribute to increasing the spread of results.[20] Nevertheless, considering the low coefficient of variation calculated for each experimental set, the obtained measures prove reasonably accurate.

There is good correspondence between in-house measures and those obtained in MTS[TM] laboratories: this confirms the validity of the testing setup and correction methods used. The best correspondence in terms of strain at maximum stress was found for PLA flat-built and side-built samples, though standing-built PLA and XTCF-20 were acceptably accurate as well, in spite of a greater variability of results. Maximum stress is often underestimated by the in-house measures, which is probably due to the poor

control over the elongation speed. Upgrade to a motor-driven electronically controlled system has already been planned: though adding a little extra cost, the expected improvement in the quality of results will definitely pay for the effort.

The test-rig presented in this paper is definitely cheaper than commercially available models. Testers in the 1 kN range cost €20,000 upwards, while the total cost of our machine, considering materials, instrumentation and labor, does not reach €1000. This makes it especially suitable for makers or small companies, to give them the opportunity to test their 3D-printed materials in-house.

One possible future development of this work could be to create all the structural parts of the machine through additive manufacturing. The presented design would be suitable for SLS/SLM as is, but cost and machine availability could be a big issue for the average maker. Therefore, the test-rig could be printed in plastic (FDM) or resin (SLA); however, the reduced stiffness and lower resistance of this kind of polymers requires a partial re-design of the geometry of most structural parts.

Declaration of Conflicting Interests

Funding

ORCID iD

Francesca Cosmi https://orcid.org/0000-0002-0191-2664

References

1. Huang Y. Additive manufacturing: current state, future potential, gaps. *J Manuf Sci Eng* 2015; 137 **[AQ3]**.

2. Gibson I, David W and Stucker RB. *Additive manufacturing technologies – rapid prototyping to direct digital manufacturing*. Singapore: Springer, 2010.

3. Ahn S, Montero M, Odell D, et al. Anisotropic material properties of fused deposition modeling ABS. *Rapid Prototyp J* 2002; 8: 248–257.

4. Cockalingam K, Jawahar N and Praveen J. Enhancement of anisotropic strength of fused deposited ABS parts by genetic algorithm. *Mater Manuf Process* 2016; 31: 2001–2010.

5. Dal Maso A and Cosmi F. Mechanical characterization of 3D-printed objects. *Mat Today Proc* 2018; 5: 26739–26746.

6. Le X, Akouri R, Passemato B, et al. Mechanical property testing and analysis of 3D printing objects. In: *ASME international mechanical engineering congress and exposition, proceedings (IMECE)*, Boston, MA, USA, 2016.

7. Rangisetty S and Peel L. The effect of infill patterns and annealing on mechanical properties of additively manufactured thermoplastic composites. In: *ASME 2017 conference on smart materials, adaptive structures and intelligent systems*, Kingsville, TX, USA, 2017.

8. Rybachuk M, Alice Mauger C, Fiedler T, et al. Anisotropic mechanical properties of fused deposition modeled parts fabricated by using acrylonitrile butadiene styrene polymer. *J Poly Eng* 2017; 37: 699–706.

9. Upadhyay K, Dwivedi R and Kumar Singh A. Determination and comparison of the anisotropic strengths of fused deposition modeling P400 ABS. *Adv 3D Print Addit Manufact Technol* 2017; 8: 96–115.

10. Ziemian C, Sharma M and Ziemian S. Anisotropic mechanical properties of ABS parts fabricated by fused deposition modelling. *Intech* 2014 **[AQ4]**.

11. Deng Z, Yao T, Zhang K, et al. A method to predict the ultimate tensile strength of 3D printing polylactic acid (PLA) materials with different printing orientations. *Compos Part B* 2019; 163: 393–402.

12. Garg A and Bhattacharya AS. An insight to the failure of FDM parts under tensile loading: finite element analysis and experimental study. *Int J Mech Sci* 2017; 120: 225–236.

13. UNI EN ISO 527-1: Plastics – determination of tensile properties, 2012 **[AQ5]**.

14. Cosmi F and Bernasconi A. Micro-CT investigation on fatigue damage evolution in short fibre reinforced polymers. *Compos Sci Technol* 2003; 79: 70–76.

15. Graupner N. Natural and man-made cellulose fibre-reinforced poly(lactic acid) (PLA) composites: an overview about mechanical characteristics and application areas. ▮▮ 2009; 40: 6–7 **[AQ6]**.

16. Bergstrom JS and Hayman D. An overview of mechanical properties and material modeling of polylactide (PLA) for medical applications. *Ann Biomed Eng* 2016; 44: 330–340.

17. Farah S. Physical and mechanical properties of PLA, and their functions in widespread applications – a comprehensive review. *Adv Drug Deliv Rev* 2016; 107: 367–392.

18. Welch B. The generalization of 'student's' problem when several different population variances are involved. *Biometrika* 1947; 34: 28–35.

19. Gedney R. Tensile testing basics, tips and trends, 2005 **[AQ7]**.

20. Brown R. Handbook of polymer testing: short-term mechanical tests. Shropshire: Rapra Technology, 2002.